Journal of Applied Sciences

ISSN 1812-5654

science alert

ANSInet
an open access publisher
http://ansinet.com

Journal of Applied Sciences 10 (3): 182-188, 2010
ISSN 1812-5654
© 2010 Asian Network for Scientific Information

Turbulence Models for Computations of 3D Turbulence Jet in Crossflow

[1]B. Bounegta, [2]R. Dizene, [1]M. Abdelkarim and [1]M.A. Maazouzi
[1]Department of Mechanical Engineering and Mechanics, University of Bechar, Algeria
[2]University of Science and Technology- Houari Bomediene Algiers, Algeria

Abstract: A turbulence models with the thermal effect of jets issuing into an incompressible hot cross at an angle over a turbine blade is the subject. Numerical solutions for two holes spacing and same jet issuing angles document strong to moderate secondary vortex structures spanning normal to direction of the jet. This fully three-dimensional flow field strongly influences the cooling performance of the hole-blade system. Turbulence closure is achieved with the realizable k-$^{\varepsilon}$ model. The realizable k-$^{\varepsilon}$ models yield reasonable agreement for the mean flow velocity and better predictions.

Key words: Film cooled turbine rotor, three dimensional flow field, numerical simulation, turbulence model, grid technique, realizable model, blowing rate

INTRODUCTION

Three-dimensional turbulent jets in crossflow have important engineering applications in both confined and unconfined environments. Examples of jets issuing into confined crossflow include internal cooling of turbine blades, dilution air jets in combustion chambers, jets from V/STOL. The examples of turbulent jets issuing into unconfined (semi-infinite) crossflow are even more numerous. These include discharges from cooling towers or film cooling of turbine blades (Acharya *et al*., 2001).

The interaction of cool air jets with hot crossflow generates complex flowfields which exist in a variety of industrial applications. In many of these applications, the resulting temperature downstream of the jet, the trajectory and physical path of the jet are critical design parameters. (Acharya *et al*., 2001).

The flow field for jet to crossflow interaction depends upon the ratio of the jet momentum to the crossflow momentum. For incompressible flow, this is the ratio r of mean flow velocities in the jet injection pipe and crossflow i.e., $R = U_j/U_{ef}$ where U_j and U_{ef} denote jet and crossflow velocities, respectively.

For a cool jet injected into a warm air crossflow, another important factor influencing the fluid thermal interaction downstream of the injecting hole is the jet issuing angle. Fig. 1 describes schematic control volume of hot air passing over a flat surface (turbine blade). This surface of study has a row of injection holes through which the cool air is issued at an angle α. The cool jet at

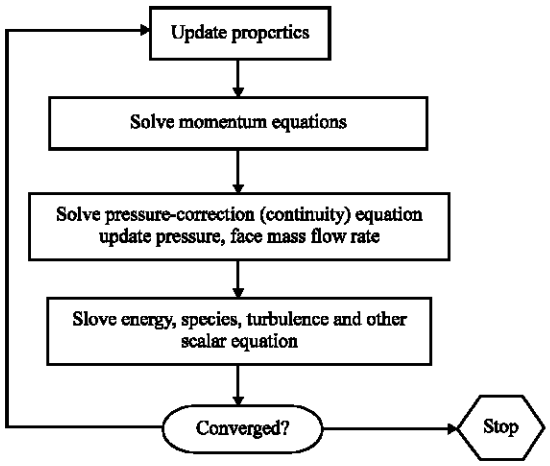

Fig. 1: Fluent schematic to solve CFD equations

T_j is injected into the hot cross-flow at T_{ef}. The injected ducts are circular pipes with radius equal to r. The injected hole formed by the intersection of the injection pipe with the wind tunnel is an ellipse with minor and major axes 2r and $D = 2r/(\cos\alpha)$, respectively. L is the distance between the hole centers.

In the near field of the film cooling jet, the dynamic large scale anisotropic structures control the mixing process. This three dimensional mixing determines the normal and transverse penetration of the jet, the accurate prediction of the jet penetration and reattachment location greatly influences the accuracy of the numerical prediction of the heat transfer process or the film cooling effectiveness on the adiabatic blade surface.

Corresponding Author: B. Bounegta, Department of Mechanical Engineering and Mechanics, University of Bechar, Algeria

COMPUTATIONAL MODEL

Heat transfer: Near the exit of the cooling jet and the film produced by the slot/hole, the heat transfer is significantly different with the rest of the part because of the mixing of the two fluid flows and the complex velocity field that will affect the convective heat transfer from the mixed fluid into the alloy.

Since, the nature of our problem involving high velocity and high heat transfer rate, the radiation and natural convection heat transfer are not considered significant and will not be accounted for in the computations.

The turbulence model will give the velocity and pressure profiles to input into energy equations. Then the convective and conductive heat transfer coefficient will be calculated from the energy equation to give the temperature profile in both the fluid and solid regions (Katotani and Golstein, 1979a). This conjugate heat transfer setup should yield more accurate result than if the convection and conduction were treated separately or independent from each other (Katotani and Golstein, 1979b).

COMPUTATIONAL METHOD

With the development of grid technique and computational methods, many researchers have investigated the characteristics of the flow filed in film cooled turbine by solving the Navier-Stockes equations. In this study, the computational tool employed in numerical simulation is the GAMBIT CFD package. The package uses the grid generation, the flow solver and the post processing software (Heschi *et al*., 2005).

The numerical scheme is used to solve the 3-D Reynolds-Averaged Navier-Stockes (RANS) equation on general structured non-orthogonal multi-grid. The numerical algorithm used Runge-Kutta scheme. A variety of convergence acceleration techniques are employed, space integration is performed using a second-order cell-centered finite volume discretization with the second and fourth-order artificial dissipation. In the following numerical simulations, a realizable k-e turbulence model with emphasis at near-wall functions will be used to predict heat transfer into an alloy flat plate and evaluate cooling film effectiveness with various different geometric configurations (Heschi *et al*., 2005).

FLUENT ANALYSIS

Fluent version 6.3.26 that utilized two or more processors was used to solve larger and more complex 3D meshes. Nevertheless, both versions should yield the same result. The meshes produced in Gambit were imported directly into Fluent. There, all boundary conditions are mapped into the mesh. The solver is segregated type, that it solves the momentum equations first to obtain velocity field. Then using these results it will solve the mass, pressure and other relevant equations. Figure 2 shows a schematic of the sequence that Fluent goes through during each iterations of the computation. The other type of solver is to couple all equation in one step. This solver could reduce computation time but it might be problematic for complex 3D equations.

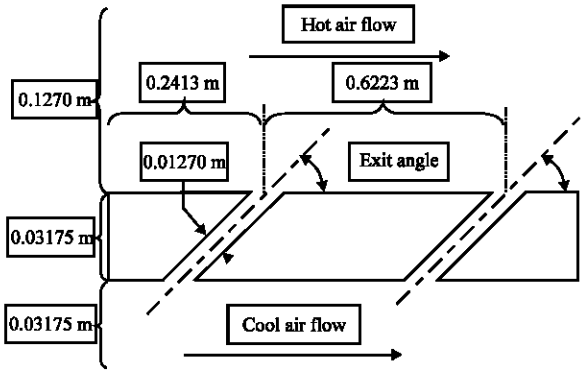

Fig. 2: General configuration of 2D model

$$-\overline{\rho u'_i u'_j} = \mu_t\left(\frac{\partial u_i}{\partial_{xj}} + \frac{\partial_{xj}}{\partial u_i}\right) - \frac{2}{3}\left(pk + \mu_t\frac{\partial u_i}{\partial_{xi}}\right)\delta_{ij} \quad (1)$$

In this project all problems were analyzed using this model. The fluent internal algorithm for this realizable turbulence model uses two transport equations for k and as follows:

$$\frac{\partial}{\partial t}(pk) + \frac{\partial}{\partial_{xj}}(pkuj) = \frac{\partial}{\partial_{xj}}\left(\left(\mu + \frac{\mu_i}{\sigma_k}\right)\frac{\partial k}{\partial x_j}\right) + G_k + G_b - p\in - Y_M + S_k \quad (2)$$

and

$$\frac{\partial}{\partial t}(p\in) + \frac{\partial}{\partial x_j}(p\in u_j) = \frac{\partial}{\partial x_j}\left(\left(\mu + \frac{\mu_t}{\sigma_e}\right)\frac{\partial \in}{\partial x_j}\right) + \rho C_1 S_e - \rho C_2\frac{\in^2}{k + \sqrt{v\in}} + C_{1e}\frac{\in}{k}C_{3e}G_b + S_e \quad (3)$$

where,

$$C_1 = \max\left(0.43, \frac{\eta}{\eta + 5}\right),\ \eta = S\frac{k}{\in},\ S = \sqrt{2S_{ij}S_{ij}} \quad (4)$$

G_k represents the generation of turbulence kinetic energy due to the mean velocity gradient.

G_b represents the generation of turbulence kinetic energy due to buoyancy, which is not important to our flows. The internal engine of Fluent may still compute this parameter since it may be difficult, if not impossible, to modify these equations.

μ_t is the eddy viscosity and computed from:

$$\mu_t = \rho C_\mu \frac{k_2}{\epsilon} \tag{5}$$

The other constants used in these fluent equations are set to suit a wide range of flow problems as recommended in Eq. 6:

$$C_{1\epsilon} = 1044,\ C_2 = 1.9,\ \sigma_k = 1.0,\ \sigma\epsilon = 1.2 \tag{6}$$

Fluent offers the option to enhance near-wall modeling integrated into the turbulence K-ε model. Near the alloy surface, the fidelity of numerical solutions is extremely important to predict accurately pressure and temperature gradients as the core turbulence flow transforms into boundary layers closer to the wall. The Thermal Effects were included in the Near-Wall Treatment for all of heat transfer problems in this project. The law-of-the-wall implemented in Fluent has a composite form:

$$T^* \equiv \frac{(T_w - T_P)\rho c_p C_\mu^{1/4} k_P^{1/2}}{\dot{q}} = \begin{cases} \Pr y^* + \frac{1}{2}\rho \Pr \frac{C_\mu^{1/4} k_P^{1/2}}{\dot{q}} U_P^2 & (y^* < y_T^*) \\ \Pr_t[\frac{1}{2}\ln(Ey^*) + P] + & \\ \frac{1}{2}\rho \frac{C_\mu^{1/4} k_P^{1/2}}{\dot{q}} \{\Pr_t U_P^2 + (\Pr - \Pr_t) U_c^2\} & (y^* > y_T^*) \end{cases} \tag{7}$$

where, P is any point in the region near the wall and given by Jayatilleke Eq. 7:

$$P = 9.24\left[\left(\frac{Pr}{Pr_t}\right)^{3/4} - 1\right]\left[1 + 0.28e^{-0.0087\,Pr/Pr_t}\right] \tag{8}$$

The wall functions in Fluent evaluate each thermal layer to determine the appropriate velocity, temperature, pressure profiles. They work well for wall-bounded flows with high Reynolds number but are limited to steady, predictable streams where there are no large pressure gradients leading to layer separations and no massive blowing or suction though the wall. Since, we expect our cooling film would not fall into these limitations such as in case with 35° exit angles with relatively acceptable velocity ratios, we believe the predictions should yield trustworthy (Brown and Saluja, 1979).

RESULTS AND DISCUSSION

The schematic of the flow domain is shown in Fig. 2. The cool jet at 150° K is injected into T_{cf} = 300°K hot cross-flow with an angle α = 35°. The injected ducts are circular pipes and interface surface duct/hole is elliptic surfaces. The mean flow velocities in the injection (inlet) plenum (0.7474 m sec^{-1}) and inlet duct are (20 m sec^{-1}), gives a moderate flow ration R = 1 for 1st case. For 2nd case the velocity ratio are R = 2 (velocity inlet plenum is 1.4949 m sec^{-1}).

The results are presented with the following structure. First, the impact of the temperature and the velocity are analyzed. Next, the contours of static temperature for different velocity ratio are examined. Finally, the findings are compared with numerical studies to show the quality of the computational method.

The flow field of jet-crossflow interaction is discussed by the analysis of the temperature and mean velocity at a velocity ratio R = 1 and R = 2.

The cooler injected air enters the system trough the plenum. Only a portion of the domain needs to be modeled because of the symmetry of the geometry. The bulk temperature of the streamwise air is 300 K and the velocity of the air stream is 20 m sec^{-1}. The bottom wall of the duct that intersect holes array is assumed to be a completely insulated (adiabatic) wall. The secondary (injected) air enters the plenum at a uniform velocity of 0.7474 m sec^{-1}. The temperature of the injected air (Tinject) is 150 K.

Figure 3-8 shows the temperature distribution of the duct length at different locations along the centerline of the middle hole (Z = 0) on the pressure side for different velocity ratio (R = 1 and R = 2).

The big blowing ratio and jet angle of 35°, more jet penetrates into the mainstream.

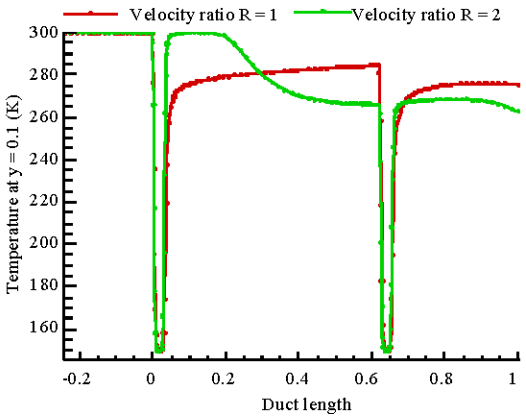

Fig. 3: Variation of the temperature at y = 0.1 versus duct length for VR = 1 and VR = 2

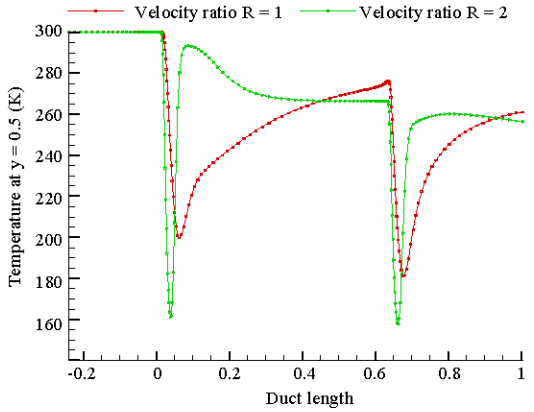

Fig. 4: Variation of the temperature at y = 0.5 versus duct length for VR = 1 and VR = 2

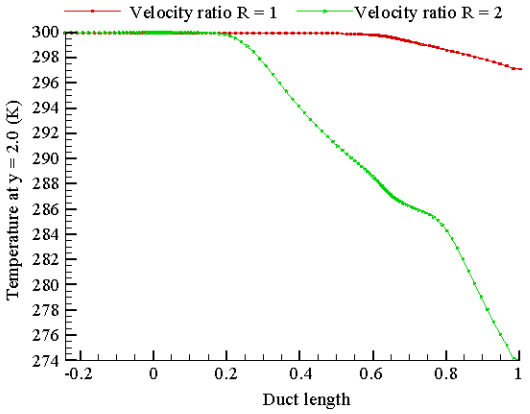

Fig. 7: Variation of the temperature at y = 2.0 versus duct length for VR = 1 and VR = 2

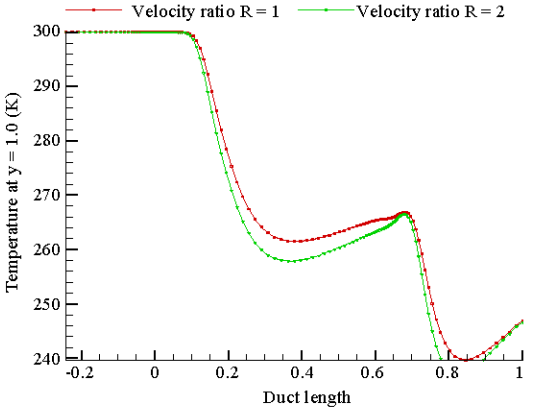

Fig. 5: Variation of the temperature at y = 1.0 versus duct length for VR = 1 and VR = 2

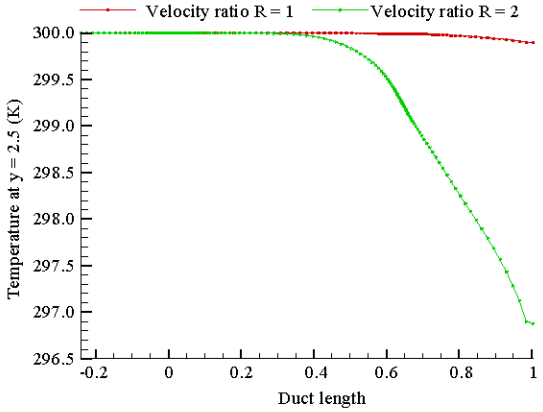

Fig. 8: Variation of the temperature at y = 2.5 versus duct length for VR = 1 and VR = 2

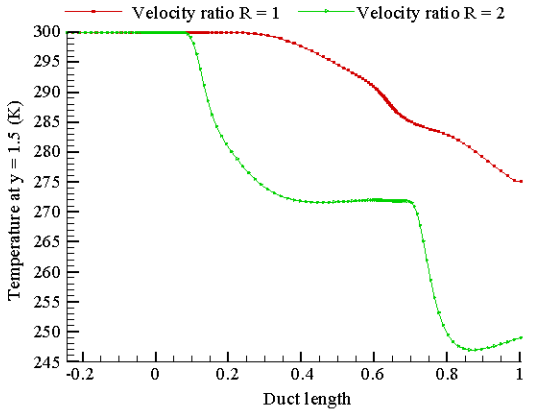

Fig. 6: Variation of the temperature at y = 1.5 versus duct length for VR = 1 and VR = 2

Figure 3-8 show the computed temperature profile along x-direction before and after cooling slot. This parametric distance is where the cooling film effectiveness is dominant. After that, the cooling jet starts to get mixed with the main stream and the temperature starts to increase faster.

Figure 5 shows the same profiles temperature at position (y = 1.5) for different velocity ratio. For y <1.5 the temperature for R =2 is important that for R = 1.

In Fig. 9-14, profiles of the streamwise velocity are shown for two velocity ratios R = 1 and R = 2. The profiles are illustrated in the spanwise symmetry plane (Z=0) at different streamwise locations (y = 0.1, 0.5, 1, 1.5, 2 and 2.5). The location y = 0 corresponds to insulate flat plate. For y≈1.5, the same velocity is obtained for two velocity ratio R = 1 and R = 2.

A higher injection rate leads to a higher penetration of the jet in the cross flow with an associated reduction of the film cooling effect due to the injection of cross flow fluid under the jets. Vorticity transport associated with the dominant vertical structure of Twin

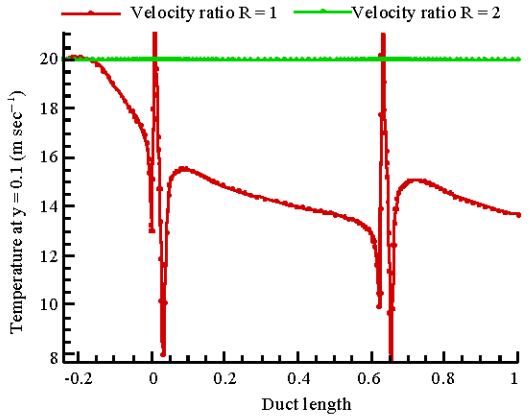

Fig. 9: Variation of the volocity magnitude at y = 0.1 versus duct length for VR = 1 and VR = 2

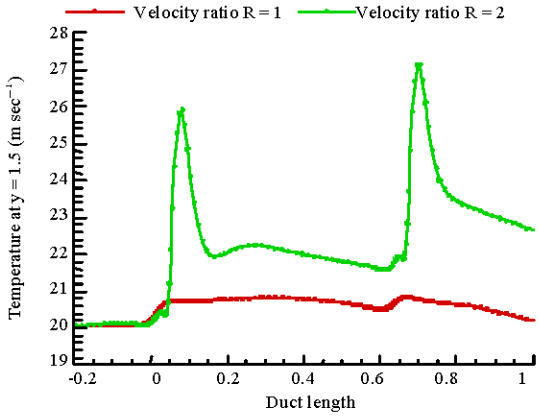

Fig. 12: Variation of the volocity magnitude at y = 1.5 versus duct length for VR = 1 and VR = 2

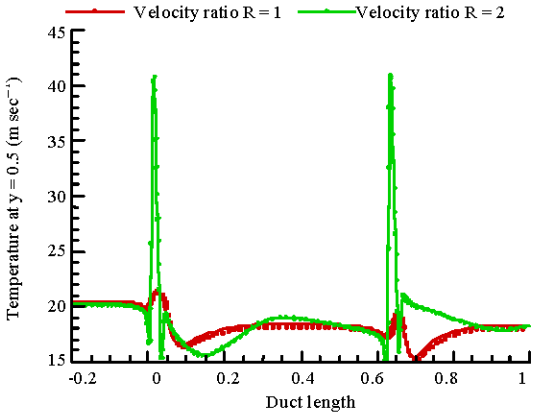

Fig. 10: Variation of the volocity magnitude at y = 0.5 versus duct length for VR = 1 and VR = 2

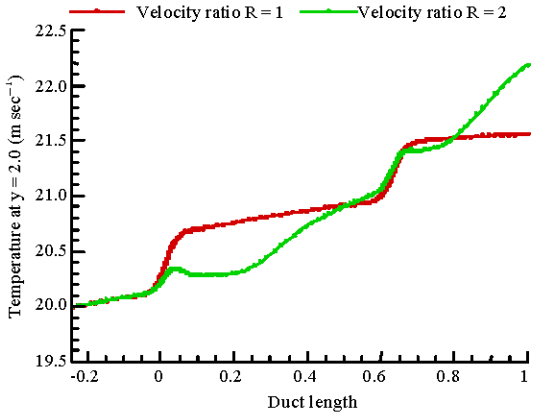

Fig. 13: Variation of the volocity magnitude at y = 2.0 versus duct length for VR = 1 and VR = 2

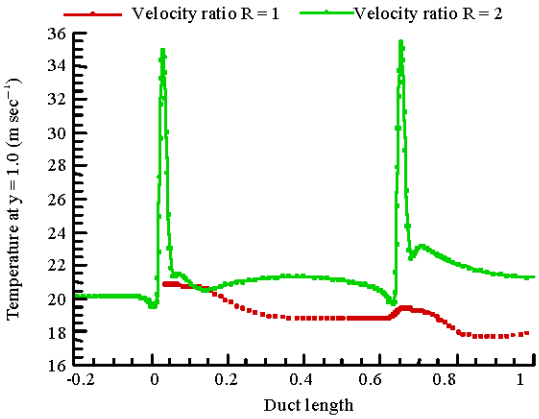

Fig. 11: Variation of the volocity magnitude at y = 1.0 versus duct length for VR = 1 and VR = 2

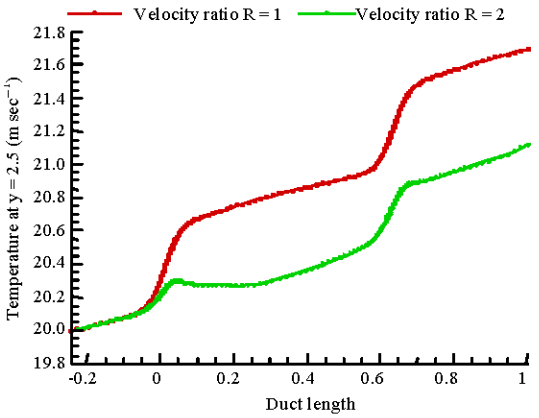

Fig. 14: Variation of the volocity magnitude at y = 2.5 versus duct length for VR = 1 and VR = 2

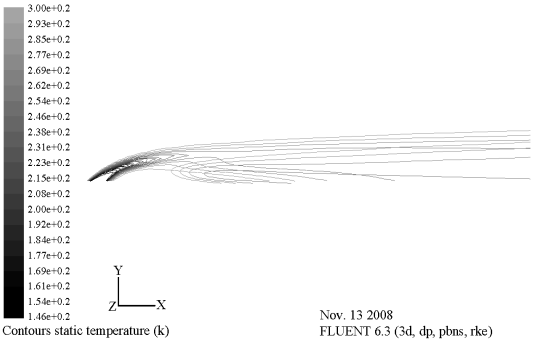

Fig. 15: Contour static temperature in symmetry plane at velocity ratio R = 1 (first hole exit domain)

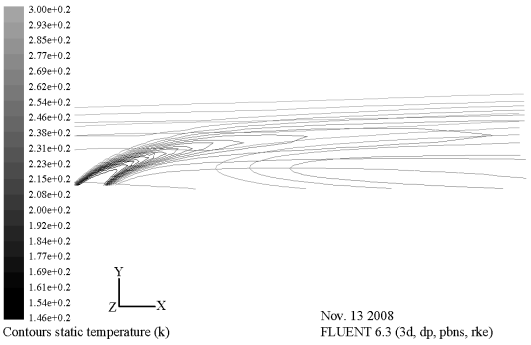

Fig. 16: Contour static temperature in symmetry plane at velocity ratio R = 1 (second hole exit domain)

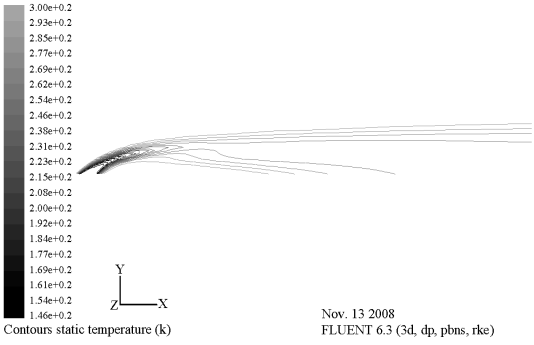

Fig. 17: Contour static temperature in symmetry plane at velocity ratio R = 2 (first hole exit domain)

Jets in CrossFlow. 14th Australasian Fluid Mechanics Conference Adelaide University, Adelaide, Australia, 10-14 December 2001.

The jet fluid with the incoming boundary layer flow which also reduces the film cooling (Fig. 15-18) (Leylek and Zerkla, 1994).

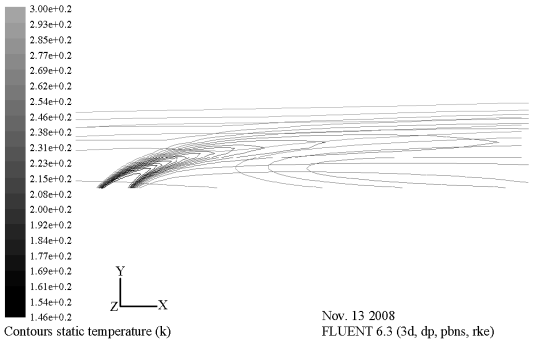

Fig. 18: Contour static temperature in symmetry plane at velocity ratio R = 2 (second hole exit domain)

CONCLUSION

An increase in freestream turbulence intensity was then shown.

The dynamical behavior of the coherent structures must therefore be incorporated in a turbulence model for the modeled predictions to reproduce the correct physics. This is therefore, the challenge to be faced by the turbulence modelers.

NOMENCLATURE

D	:	Film Cooling Hole Diameter (m)
L	:	Film Cooling Delivery Length (m)
Pr	:	Prandtl Number
Re_D	:	Eynolds Number based on Hole Diameter and Bulk Coolant Velocity
T	:	Temperature (K)
TI	:	Turbulence Intensity (%)
u	:	Streamwise Component of Velocity (m sec^{-1})
U_0	:	Verage Freestream Velocity (m sec^{-1})
U_c	:	Ulk Coolant Velocity (m sec^{-1})
R	:	Jet to mainstream velocity ratio
TBC	:	Thermal barrier coating
c_p	:	Pecific heat at constant pressure (J/kg-K)
K	:	Thermal conductivity (W/m-k)
t	:	Time (sec)
W	:	Spanwise component of velocity (m sec^{-1})
X	:	Streamwise distance from center of cooling hole (m)
Y	:	Normal distance from alloy wall surface (m)
Z	:	Spanwise distance from center of cooling hole (m)
α	:	Film hole injection angle or exit angle (°)
ρ	:	Density (kg m^{-3})
μ	:	Viscosity (kg m sec^{-1})

REFERENCES

Acharya, S., M. Tyagi and A. Hoda, 2001. Flow and heat transfer predictions for film cooling. Ann. New York Acad. Sci., 934: 110-125.

Brown, A. and C.L. Saluja, 1979. Film cooling from a single hole and a row of holes of variable pitch to diameter ratio. Int. J. Heat Mass Tran., 22: 525-533.

Heschi, C., W. Sanz and P. Klanatsky, 2005. Implementation and comparison of different turbulence models for three dimensional wall jets with FLUENT. CFD Forum 2005, Bad Nauheim, Deutschland, pp: 1-34. http://www.fh-pinkafeld.ac.at/fhplus/eum/pdf/CFD_Forum2005_Part_I.pdf.

Katotani, K. and R.J. Golstein, 1979a. On the nature of jet entering a turbulent flow–part A-jet mainstream interaction. ASME J. Eng. Power, 101: 459-465.

Katotani, K. and R.J. Golstein, 1979b. On the nature of jet entering a turbulent flow–part B-film cooling performance. ASME J. Eng. Power, 101: 466-470.

Leylek, J.H. and R.D. Zerkle, 1994. Discrete jet film cooling: A comparison of computational results with experiments. ASME J. Turbomachinery, 116: 358-368.